

Electron-phonon coupling in the charge density wave state of CsV₃Sb₅

Yaofeng Xie,^{1,*} Yongkai Li,^{2,3,4,*} Philippe Bourges,^{5,†} Alexandre Ivanov,⁶ Zijin Ye,⁷ Jia-Xin Yin,⁸
M Zahid Hasan,⁸ Aiyun Luo,⁷ Yugui Yao,^{2,3} Zhiwei Wang,^{2,3,4,‡} Gang Xu,⁷ and Pengcheng Dai^{1,§}

¹*Department of Physics and Astronomy, Rice University, Houston, Texas 77005, USA*

²*Centre for Quantum Physics, Key Laboratory of Advanced Optoelectronic Quantum Architecture and Measurement (MOE),
School of Physics, Beijing Institute of Technology, Beijing 100081, China*

³*Beijing Key Lab of Nanophotonics and Ultrafine Optoelectronic Systems,
Beijing Institute of Technology, Beijing 100081, China*

⁴*Material Science Center, Yangtze Delta Region Academy of Beijing Institute of Technology, Jiaxing, 314011, China*

⁵*Laboratoire Léon Brillouin, CEA-CNRS, Université Paris-Saclay, CEA Saclay, 91191 Gif-sur-Yvette, France*

⁶*Institut Laue-Langevin, 71 avenue des Martyrs CS 20156, 38042 Grenoble Cedex 9, France*

⁷*Wuhan National High Magnetic Field Center & School of Physics,
Huazhong University of Science and Technology, Wuhan 430074, China*

⁸*Laboratory for Topological Quantum Matter and Advanced Spectroscopy (B7),
Department of Physics, Princeton University, Princeton, New Jersey 08544, USA*

(Dated: November 2, 2021)

Metallic materials with kagome lattice structure are interesting because their electronic structures can host flat bands, Dirac cones, and van Hove singularities, resulting in strong electron correlations, nontrivial band topology, charge density wave (CDW), and unconventional superconductivity. Recently, kagome lattice compounds AV₃Sb₅ ($A = \text{K, Rb, Cs}$) are found to have intertwined CDW order and superconductivity. The origin of the CDW has been suggested to be purely electronic, arising from Fermi-surface instabilities of van Hove singularity (saddle point) near the M points. Here we use neutron scattering experiments to demonstrate that the CDW order in CsV₃Sb₅ is associated with static lattice distortion and a sudden hardening of the B_{3u} longitudinal optical phonon mode, thus establishing that electron-phonon coupling must also play an important role in the CDW order of AV₃Sb₅.

Two-dimensional (2D) correlated transition metal materials with nearly square lattice structures have been heavily investigated because they display exotic properties such as unconventional superconductivity, electronic nematic phase, and intertwined charge, spin, and lattice order [1, 2]. The 2D kagome lattice metallic materials, where atoms are arranged into layered sets of corner-sharing triangles [3], are interesting because their electronic structures can host flat bands with quenched kinetic energy [4–7], Dirac cones [8, 9], and van Hove singularities, resulting in strong electron correlations, nontrivial band topology, charge density wave (CDW) [10–12], and unconventional superconductivity [13, 14]. Recently, CDW order and superconductivity have been discovered to coexist in kagome lattice metals AV₃Sb₅ ($A = \text{K, Rb, Cs}$) [Figs. 1(a,b)] [14–16]. In general, CDW order may originate from Fermi-surface instability following the Peierls’ description of an electronic instability in a one-dimensional chain of atoms [17–20] or strong electron phonon coupling (EPC)/electron-electron correlations [21–23]. Using inelastic X-ray scattering and angle resolved photoemission spectroscopy (ARPES), it was found that the CDW here may have purely electronic origin arising from Fermi-surface instabilities of van Hove singularity (saddle point) near the M points without the involvement of lattice and electron-phonon coupling [Figs. 1(c) and 2(a)] [24]. If this is indeed the case [25, 26], the CDW order and superconductivity may intertwine in AV₃Sb₅ to form the exotic roton

pair-density wave superconductivity and Majorana zero mode [16, 27, 28]. Therefore, to understand the electron pairing mechanism of superconductivity in AV₃Sb₅, one must first unveil the microscopic origin of the CDW order.

A CDW order resulting from a pure electronic origin via Fermi surface nesting should not distort the crystalline lattice or exhibit phonon anomaly, as suggested from inelastic X-ray scattering experiments [24]. However, recent ARPES [29] and optical spectroscopy [30] measurements in AV₃Sb₅ suggest that the momentum dependent EPC plays an important role in inducing the CDW transition. Since neutrons cannot detect translational symmetry-breaking electron charge distribution but are sensitive to lattice distortion and phonon anomaly induced by the CDW order, we use neutron scattering to confirm the charge order and search for phonon anomaly across the CDW order temperature.

In this paper, we report elastic and inelastic neutron scattering studies of CsV₃Sb₅, which exhibits CDW order at $T_{CDW} = 94$ K and superconductivity at $T_c = 2.5$ K [14]. We observe in-plane 2 by 2 superlattice peak below $T_{CDW} = 94$ K, thus revealing that the CDW order in CsV₃Sb₅ is associated with lattice distortion and not a pure electronic instability [20, 23]. However, we find no detectable changes in charge ordering intensity across T_c . Furthermore, we use inelastic neutron scattering to map out longitudinal acoustic and optical phonon modes near Bragg peak position (3, 0, 0) at temperatures across

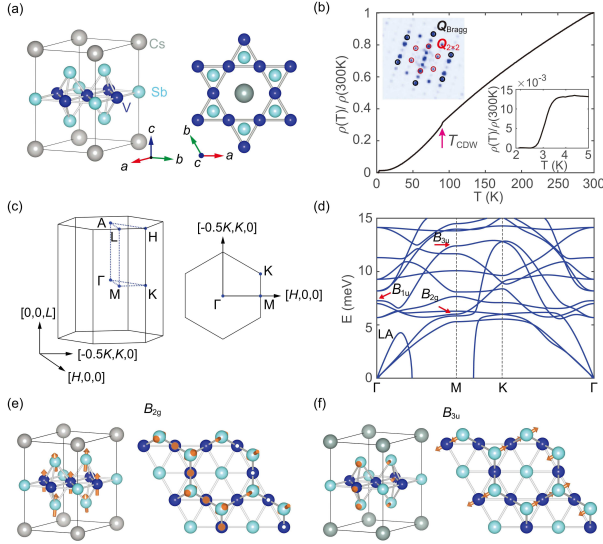


FIG. 1. (a) Crystal structure of CsV_3Sb_5 from three-dimensional view (left) and top view (right). (b) Temperature dependence of resistivity of CsV_3Sb_5 , where CDW order is seen around 95 K marked by the arrow. The upper inset is the Fourier transform of Sb topographic image from STM measurement, showing the ordering peaks ($Q_{2\times 2}$) and Bragg peaks (Q_{Bragg}) [15]. The lower inset shows superconducting transition temperature of the sample. (c) 3D and 2D Brillouin zone of CsV_3Sb_5 . The high symmetry points are specified. (d) DFT calculated phonon spectra of CsV_3Sb_5 . Full vanadium breathing vibration associated with the B_{1u} mode is marked by the arrow around 7 meV [see Fig. 4(a)]. The B_{2g} and B_{3u} modes at the M point are labeled. Lattice distortion for the B_{2g} (e) and B_{3u} (f) modes at the M point in three-dimensional view (left) and top view (right).

T_{CDW} and T_c (Figs. 1-4). While acoustic phonon mode show no dramatic change across T_{CDW} consistent with the earlier work by inelastic X-ray scattering [24], we find that optical phonon mode with B_{3u} symmetry [Fig. 1(d,f)], possibly associated with the 2 by 2 charge order and inverse Star of David deformation of the kagome lattice [31–34], hardens across T_{CDW} at the M point. We also identified an optical phonon mode near the expected energy for the phonon mode with B_{1u} symmetry at Γ point [Fig. 1(d)], and found it to have no observable changes across T_{CDW} . Therefore, our results firmly establish that the CDW order in CsV_3Sb_5 is not a purely electronic transition, and the EPC must also play an important role in the formation of CDW order.

Our neutron scattering experiments were carried out at the IN8 thermal triple-axis spectrometer at the Institut Laue-Langevin (ILL), Grenoble, France. We used doubly focused pyrolytic graphite monochromator and analyzer with PG(0,0,2) reflection and fixed scattered (final) energy $E_f = 14.68$ meV. Several scans have been performed with a 2D-focusing Si(1,1,1) monochromator. Using a hexagonal lattice with $a = b = 5.495$ Å, $c = 9.309$ Å as shown in Fig. 1(a) to describe its crystal structure, the

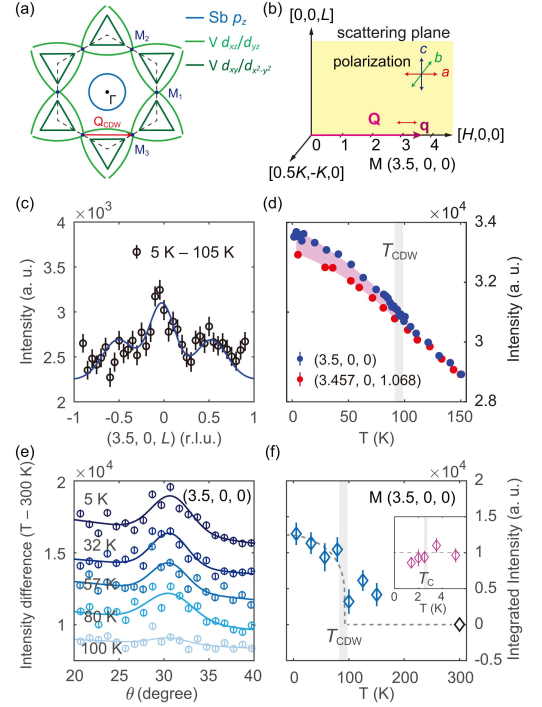


FIG. 2. (a) Schematics of the Fermi surface of CsV_3Sb_5 , where the circular Fermi surface near Γ is from Sb p_z band, and vanadium d_{xz}/d_{yz} and $d_{xy}/d_{x^2-y^2}$ bands are shown in light and dark green, respectively [14, 26, 29]. The CDW order is suggested to be associated with Fermi surface instability of the M points (red arrow). (b) Schematics of the $[H, 0, L]$ scattering plane. The double-headed arrows represent the phonon polarization directions. For wave vectors probed in the present experiment, we are mostly probing longitudinal phonon modes along the Γ - M (H) direction. (c) The temperature difference elastic scattering along the $[3.5, 0, L]$ direction. The raw data is shown in the supplementary information. The solid line is the Gaussian fit to the data. (d) Temperature dependence of the scattering at $(3.5, 0, 0)$ and $(3.475, 0, 1.068)$ positions [35]. (e) Temperature differences of rocking curve scans across $\mathbf{Q} = (3.5, 0, 0)$ using 300 K data as background. The solid lines are Gaussian fits to the data. (f) Temperature dependence of the integrated intensity at $(3.5, 0, 0)$ across the T_{CDW} . The inset shows temperature dependence of the CDW order integrated intensity across T_c .

momentum transfer $\mathbf{Q} = H\mathbf{a}^* + K\mathbf{b}^* + L\mathbf{c}^*$ is denoted as (H, K, L) in reciprocal lattice units (r.l.u.) [Fig. 1(c)] [14]. About four hundred individual single crystals were co-aligned on four aluminum plates to form an assembly with a volume of 0.11 cm³ and an in-plane mosaic spread of 3.5 degrees [35]. The crystal assembly was put inside a He cryostat and oriented in the $[H, 0, L]$ horizontal scattering plane. We also use density functional theory (DFT) to calculate the phonon spectra similarly to previous work [31].

Figure 1(b) shows transport data for CsV_3Sb_5 , confirming the existence of CDW order below $T_{CDW} = 95$ K and superconductivity below $T_c \approx 2.5$ K. Previous

scanning tunneling microscopy results showing 2 by 2 charge ordering is shown in the upper inset [15]. Figures 1(d,e,f) summarize DFT calculated phonon spectra at ambient pressure and the symmetries of the most interesting modes near the M point in reciprocal space. Consistent with the previous work [31], we find that the longitudinal acoustic phonon mode is unstable at ambient pressure, suggesting that this mode may be relevant to the formation of CDW order. At the Brillouin zone boundary M point, we expect to observe optical phonon modes with B_{2g} and B_{3u} symmetry, corresponding to out of plane and half breathing mode of vanadium as shown in Figs. 1(e) and 1(f), respectively.

Figure 2 summarizes the key results from our neutron diffraction experiments to probe the temperature dependence of the lattice distortion induced by the CDW order. From ARPES experiments, it was found that the electronic structure of AV_3Sb_5 is dominated by vanadium bands near M points [Fig. 2(a)] [14, 29, 36]. Therefore, the 2 by 2 CDW order may arise from Fermi surface nesting of quasiparticle excitations between three M points. Since our crystal assembly is aligned in the $[H, 0, L]$ scattering zone [Fig. 2(b)], we can probe elastic scattering as well as phonons around nuclear Bragg peak $(3, 0, 0)$ (Γ) position. Figure 2(c) shows temperature difference plot of the $[3.5, 0, L]$ elastic scan between 5 K and 100 K. We find a clear peak centered at $L = 0$ and weaker peaks at $L = \pm 0.5$, thus establishing the presence of low-temperature lattice distortion in CsV_3Sb_5 . To confirm that the temperature dependent lattice distortion is associated with CDW order [14–16, 24], we measure temperature dependence of the scattering at the $(3.5, 0, 0)$ (signal) and $(3.457, 0, 1.068)$ (background) positions, revealing clear intensity gain of the $(3.5, 0, 0)$ scattering approximately below T_{CDW} [Fig. 2(d)]. Figure 2(e) shows rocking curve scans around $(3.5, 0, 0)$ at temperatures across T_{CDW} using 300 K data as background scattering. While the scattering is featureless at 100 K, a clear peak centered at $(3.5, 0, 0)$ appears at temperatures below T_{CDW} [Figure 2(e)]. Figure 2(f) shows temperature dependence of the integrated intensity, again confirming the appearance of the CDW peak below T_{CDW} . However, the intensity of CDW peak does not seem to change across the superconducting transition temperature T_c [see inset of Fig. 2(f)].

Figures 3(a) and 3(b) show constant- \mathbf{Q} scans at $\mathbf{Q} = (2.5, 0, 0)$ (the M point) and $(2.7, 0, 0)$ (approximate middle of the Brillouin zone), respectively, from room temperature to 5 K across T_{CDW} . These scans show two weakly dispersive phonon modes at $E \approx 6$ meV and ~ 10 meV. While the ~ 10 meV mode at the M point shows a clear ~ 2 meV hardening below T_{CDW} , the ~ 6 meV mode only hardens slightly on cooling, and has negligible changes across T_{CDW} [Fig. 3(c)]. Similar behavior is seen in the full-width-half-maximum (FWHM) of the ~ 10 meV mode, but not the ~ 6 meV mode [Fig. 3(e)] For

comparison, these two phonon modes at $\mathbf{Q} = (2.7, 0, 0)$ show no observable anomaly across T_{CDW} in energy position [Fig. 3(d)] and width [Fig. 3(f)]. The wave vector dependence of the FWHM of the ~ 6 meV and ~ 10 meV modes at temperatures above (100 K and 300 K) and below (5 K) T_{CDW} is shown in Figs. 3(g) and 3(h). Consistent with Figs. 3(a-f), the ~ 10 meV mode shows clear broadening below T_{CDW} at the M point.

To understand the microscopic origin of the observed phonon spectra, we compare the data in Fig. 3 with the phonon spectra calculated from DFT [Figs. 4(a,d,e)]. Figure 4(b) shows constant- \mathbf{Q} scans at $\mathbf{Q} = (3, 0, 0)$ zone center below and above T_{CDW} , revealing a clear phonon mode at $E \approx 11$ meV. Temperature independence of the mode energy between 5 K and 300 K shown in Fig. 4(c) suggests that the mode is not obviously affected by the CDW order at 95 K. Therefore, we conclude that this phonon mode is irrelevant to the CDW order. Comparing energy of the observed mode with DFT calculation under 5 GPa [Fig. 4(d)], we conclude that the 11 meV mode is likely to be the optical phonon mode with B_{1u} symmetry [Figs. 4(a)]. Figure 4(e) compares the measured and calculated dispersion curves for CsV_3Sb_5 . Inspection of the Figure reveals that the measured longitudinal acoustic phonon mode agrees with the DFT calculation unfolded in the CDW state reasonably well. This means that the energy of the zone boundary longitudinal acoustic phonon mode occurs at approximately 6 meV. Since temperature dependence of the mode energy shows a slight hardening below T_{CDW} [Fig. 3(c)], our results indicate no softening of the acoustic phonon modes at the M point in the CDW state, consistent with the inelastic X-ray scattering work [24]. On the other hand, the optical phonon mode at ~ 10 meV is likely associated with half breathing mode of vanadium with B_{3u} symmetry [Fig. 4(e)].

As discussed in Ref. [23], the classical picture of Fermi surface nesting induced CDW order from Peierls' description [17, 18] fails in many real systems and the wave vector dependence of the EPC matrix element determines the characteristic of the CDW phase. For example, CDW order in $NbSe_2$ is not due to Fermi surface nesting but instead arises from the EPC as it is seen phonon energy softening, broadened phonon line-width at the CDW ordering wave vector [23]. The situation in CsV_3Sb_5 is somewhat different. While there is no evidence of acoustic phonon softening and broadening at the charge ordering wave vector (Figs. 3 and 4) consistent with the weakly first order nature of the CDW transition [14, 24], the energy of optical phonon mode with B_{3u} symmetry shows a clear hardening below T_{CDW} [Fig. 3(c)]. In addition, the optical phonon line-width broadens at the CDW wave vector below T_{CDW} [Fig. 3(h)]. Since charge order occurs at three equivalent M points, superposition of three B_{3u} modes by band folding in the CDW state can lead to an inverse Star of David deformation

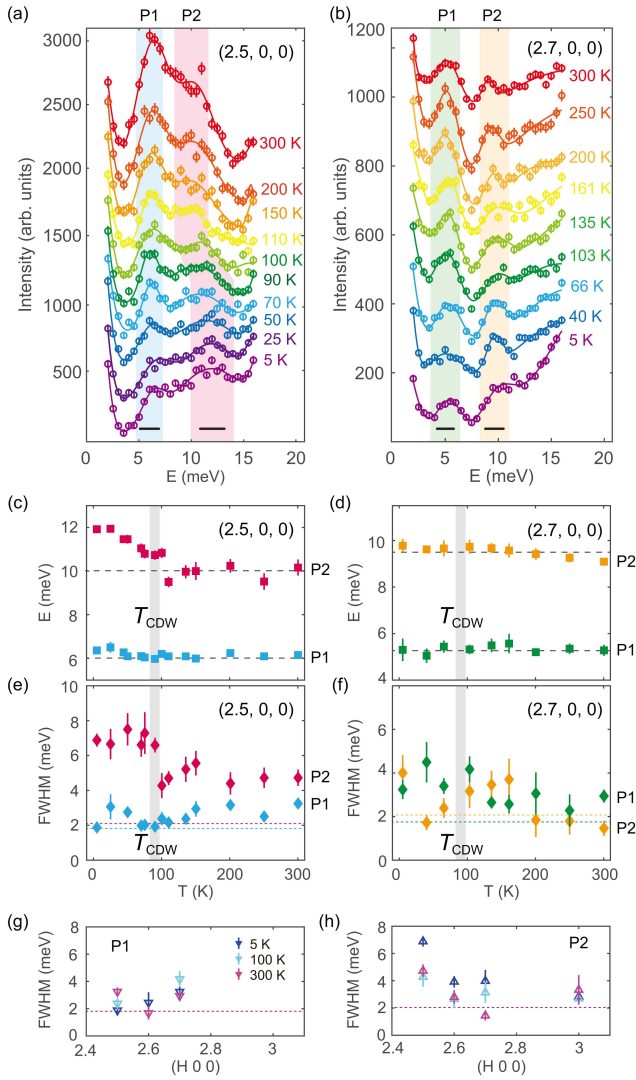


FIG. 3. (a,b) Temperature dependence of the constant- \mathbf{Q} scans at $\mathbf{Q} = (2.5, 0, 0)$ and $(2.7, 0, 0)$, respectively. The color-shaded regions highlight the two peaks, P1 and P2, observed by inelastic neutron scattering. Solid lines are results from multiple Gaussian fits. The scans are shifted vertically for clarity. The horizontal bars indicate instrumental energy resolution at different energies. (c,d) Temperature dependence of the phonon energy at $(2.5, 0, 0)$ and $(2.7, 0, 0)$, respectively. The phonon mode at $\mathbf{Q} = (2.5, 0, 0)$ hardens below T_{CDW} . (e,f) Temperature dependent phonon energy line-widths of the P1 and P2 mode at $(2.5, 0, 0)$ and $(2.7, 0, 0)$, respectively. (g,h) Wave vector dependence of the phonon line-widths of the P1 and P2 modes, respectively. The shaded vertical bars in (c-f) mark the temperature of CDW order in CsV_3Sb_5 and horizontal dashed lines are guides to the eye.

of a vanadium breathing mode with A_{1g} symmetry and two other degenerate modes that do not have three fold rotational symmetry [Figs. 4(f,g)]. Therefore, our results provide strong evidence that the EPC must play an important role in the formation of the CDW order in CsV_3Sb_5 . Although recent μSR measurements suggest

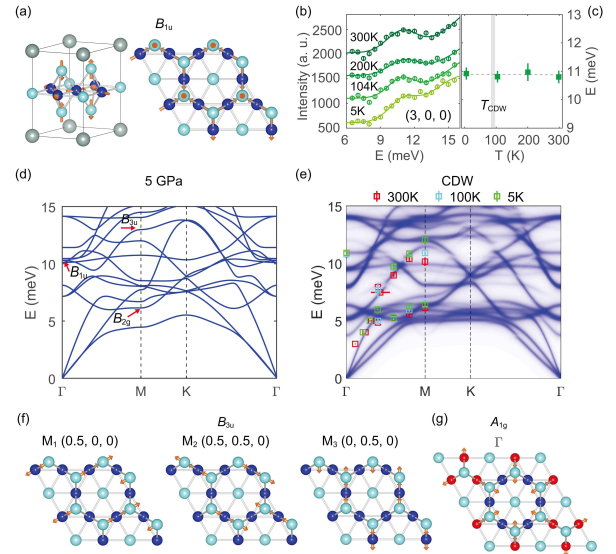


FIG. 4. (a) Lattice distortion of the full breathing mode with the B_{1u} symmetry at the Γ point in three-dimensional view (left) and top view (right). (b) Temperature dependence of the constant- \mathbf{Q} scans at $(3, 0, 0)$, where a phonon mode at 11 meV is seen. The solid lines are Gaussian fits to the data. The scans are shifted vertically for clarity. (c) Temperature dependence of the phonon mode energy at $(3, 0, 0)$. (d) DFT calculated phonon spectra at a hydrostatic pressure of 5 GPa. The B_{1u} mode at the Γ point is labeled. We note that the B_{1u} mode energy is shifted from 7 meV at 0 GPa to 11 meV at 5 GPa. (e) Comparison of DFT calculated phonon spectra in the CDW phase with inelastic neutron scattering determined phonon dispersions measured at 5, 100, and 300 K. The calculation is unfolded to the non-CDW phase to compare with the neutron data. (f) Vanadium vibrational mode with B_{3u} symmetry at three M positions. (g) Sum of the three B_{3u} modes has A_{1g} symmetry at Γ point in the CDW state.

that CDW order is also associated with a time reversal symmetry breaking field [37], consistent with the presence of a chiral flux phase in the CDW state of CsV_3Sb_5 [38, 39], it is unclear how the time reversal symmetry breaking field in the CDW state induced by flux phase can affect the lattice and its vibrations.

In summary, we have carried out elastic and inelastic neutron scattering experiments on CsV_3Sb_5 . Our elastic results confirm the presence of 2 by 2 charge order below 95 K, indicating that the CDW order also involves lattice distortion. By comparing phonons measured by inelastic neutron scattering experiments with that of DFT calculations, we conclude that acoustic phonons in CsV_3Sb_5 do not respond to CDW order but optical phonon mode with B_{3u} symmetry hardens below T_{CDW} at M points. This phonon hardening is likely associated with an inverse Star of David deformation of a vanadium atoms with A_{1g} symmetry [31]. These results therefore indicate that the effect of lattice must be taken into account to achieve a comprehensive understanding of the CDW state in AV_3Sb_5 .

P.D. is grateful to Binghai Yan, B. R. Ortiz, and Stephen Wilson for helpful discussions. The neutron scattering and basic materials characterization work at Rice is supported by the U.S. Department of Energy, BES under Grant No. DE-SC0012311 and by the Robert A. Welch Foundation under Grant No. C-1839, respectively (P.D.). The work at Beijing Institute of Technology was supported by the National Key R&D Program of China (Grant No. 2020YFA0308800), the National Science Foundation of China (Grant Numbers. 92065109, 11734003), the Beijing Natural Science Foundation (Grant No. Z190006, Z210006), and the Beijing Institute of Technology (BIT) Research Fund Program for Young Scholars (Grant No. 3180012222011). Z.W. thanks the Analysis & Testing Center at BIT for assistance in facility support. Work at Huazhong University of Science and Technology was supported by the National Key Research and Development Program of China (2018YFA0307000), and the National Natural Science Foundation of China (11874022). Work at Princeton University was supported by the U.S. Department of Energy under Grant No. DOE/BES DEFG-02-05ER46200.

* These authors made equal contributions to this work.

† philippe.bourges@cea.fr

‡ zhiweiwang@bit.edu.cn

§ pdai@rice.edu

- [1] E. Fradkin, S. A. Kivelson, and J. M. Tranquada, *Rev. Mod. Phys.* **87**, 457 (2015).
- [2] P. C. Dai, *Rev. Mod. Phys.* **87**, 855 (2015).
- [3] I. Syôzi, *Progress of Theoretical Physics* **6**, 306 (1951).
- [4] B. Sutherland, *Phys. Rev. B* **34**, 5208 (1986).
- [5] D. Leykam, A. Andreanov, and S. Flach, *Advances in Physics: X* **3**, 1473052 (2018).
- [6] I. I. Mazin, Harald O. Jeschke, Frank Lechermann, Hunpyo Lee, Mario Fink, Ronny Thomale, and Roser Valentí, *Nat. Comm.* **5**, 4261 (2014).
- [7] Jia-Xin Yin, Songtian S Zhang, Guoqing Chang, Qi Wang, Stepan S Tsirkin, Zurab Guguchia, Biao Lian, Huibin Zhou, Kun Jiang, Ilya Belopolski, Nana Shumiya, Daniel Multer, Maksim Litskevich, Tyler A Cochran, Hsin Lin, Ziqiang Wang, Titus Neupert, Shuang Jia, Hechang Lei, and M Zahid Hasan, *Nat. Phys.* **15**, 443 (2019).
- [8] Linda Ye, Mingu Kang, Junwei Liu, Felix von Cube, Christina R. Wicker, Takehito Suzuki, Chris Jozwiak, Aaron Bostwick, Eli Rotenberg, David C. Bell, Liang Fu, Riccardo Comin, and Joseph G. Checkelsky, *Nature* **555**, 638 (2018).
- [9] Jia-Xin Yin, Songtian S. Zhang, Hang Li, Kun Jiang, Guoqing Chang, Bingjing Zhang, Biao Lian, Cheng Xiang, Ilya Belopolski, Hao Zheng, Tyler A. Cochran, Su-Yang Xu, Guang Bian, Kai Liu, Tay-Rong Chang, Hsin Lin, Zhong-Yi Lu, Ziqiang Wang, Shuang Jia, Wenhong Wang, and M. Zahid Hasan, *Nature* **562**, 91 (2018).
- [10] Shun-Li Yu and Jian-Xin Li, *Phys. Rev. B* **85**, 144402 (2012).
- [11] Wan-Sheng Wang, Zheng-Zhao Li, Yuan-Yuan Xiang, and Qiang-Hua Wang, *Phys. Rev. B* **87**, 115135 (2013).
- [12] Maximilian L. Kiesel, Christian Platt, and Ronny Thomale, *Phys. Rev. Lett.* **110**, 126405 (2013)
- [13] B. R. Ortiz, L. C. Gomes, J. R. Morey, M. Winiarski, M. Bordelon, J. S. Mangum, I. W. H. Oswald, J. A. Rodriguez-Rivera, J. R. Neilson, S. D. Wilson, E. Ertekin, T. M. McQueen, and E. S. Toberer, *Phys. Rev. Mater.* **3**, 094407 (2019).
- [14] B. R. Ortiz, S. M. Teicher, Y. Hu, J. L. Zuo, P. M. Sarte, E. C. Schueller, A. M. Abeykoon, M. J. Krogstad, S. Rosenkranz, R. Osborn, R. Seshadri, L. Balents, J. He, and S. D. Wilson, *Phys. Rev. Lett.* **125**, 247002 (2020).
- [15] Yu-Xiao Jiang, Jia-Xin Yin, M. Michael Denner, Nana Shumiya, Brenden R. Ortiz, Gang Xu, Zurab Guguchia, Junyi He, Md Shafayat Hossain, Xiaoxiong Liu, Jacob Ruff, Linus Kautzsch, Songtian S. Zhang, Guoqing Chang, Ilya Belopolski, Qi Zhang, Tyler A. Cochran, Daniel Multer, Maksim Litskevich, Zi-Jia Cheng, Xian P. Yang, Ziqiang Wang, Ronny Thomale, Titus Neupert, Stephen D. Wilson, and M. Zahid Hasan, *Nature Materials* **20**, 1353 (2021).
- [16] Zuwei Liang, Xingyuan Hou, Fan Zhang, Wanru Ma, Ping Wu, Zongyuan Zhang, Fanghang Yu, J.-J. Ying, Kun Jiang, Lei Shan, Zhenyu Wang, and X.-H. Chen, *Phys. Rev. X* **11**, 031026 (2021).
- [17] R. E. Peierls, *Quantum Theory of Solids* (Oxford Univ. Press, New York, 1955).
- [18] W. Kohn, *Phys. Rev. Lett.* **2**, 393 (1959).
- [19] T. M. Rice and G. K. Scott, *Phys. Rev. Lett.* **35**, 120 (1975).
- [20] M. D. Johannes, I. I. Mazin, and C. A. Howells, *Phys. Rev. B* **73**, 205102 (2006).
- [21] Jan Zaanen and Olle Gunnarsson, *Phys. Rev. B* **40**, 7391(R) (1989).
- [22] C. M. Varma and A. L. Simons, *Phys. Rev. Lett.* **51**, 138 (1983).
- [23] Xuetao Zhu, Yanwei Cao, Jiandi Zhang, E. W. Plummer, and Jiandong Guo, *PNAS* **112**, 2367 (2015).
- [24] Haoxiang Li, T.T. Zhang, T. Yilmaz, Y.Y. Pai, C.E. Marvinney, A. Said, Q.W. Yin, C.S. Gong, Z.J. Tu, E. Vescovo, C.S. Nelson, R. G. Moore, S. Murakami, H.C. Lei, H.N. Lee, B. J. Lawrie, and H. Miao, *Phys. Rev. X* **11**, 031050 (2021).
- [25] Takamori Park, Mengxing Ye, and Leon Balents, *Phys. Rev. B* **104**, 035142 (2021).
- [26] Mingu Kang, Shiang Fang, Jeong-Kyu Kim, Brenden R. Ortiz, Jonggyu Yoo, Byeong-Gyu Park, Stephen D. Wilson, Jae-Hoon Park, and Riccardo Comin, arXiv:2105.01689.
- [27] Hui Chen, Haitao Yang, Bin Hu, Zhen Zhao, Jie Yuan, Yuqing Xing, Guojian Qian, Zihao Huang, Geng Li, Yuhan Ye, Sheng Ma, Shunli Ni, Hua Zhang, Qiangwei Yin, Chunsheng Gong, Zhijun Tu, Hechang Lei, Hengxin Tan, Sen Zhou, Chengmin Shen, Xiaoli Dong, Binghai Yan, Ziqiang Wang, and Hong-Jun Gao, *Nature*, DOI:10.1038/s41586-021-03983-5 (2021).
- [28] He Zhao, Hong Li, Brenden R. Ortiz, Samuel M. L. Teicher, Taka Park, Mengxing Ye, Ziqiang Wang, Leon Balents, Stephen D. Wilson, and Ilija Zeljkovic, *Nature* DOI: 10.1038/s41586-021-03946-w (2021).
- [29] Hailan Luo, Qiang Gao, Hongxiong Liu, Yuhao Gu, Dingsong Wu, Changjiang Yi, Junjie Jia, Shilong Wu, Xianguyu Luo, Yu Xu, Lin Zhao, Qingyan Wang, Hanqing

- Mao, Guodong Liu, Zhihai Zhu, Youguo Shi, Kun Jiang, Jiangping Hu, Zuyan Xu, X. J. Zhou, arxiv: 2107.02688.
- [30] E. Uykur, B. R. Ortiz, S. D. Wilson, M. Dressel, and A. A. Tsirlin, arxiv: 2103.07912.
- [31] Hengxin Tan, Yizhou Liu, Ziqiang Wang, Binghai Yan, *Phys. Rev. Lett.* **127**, 046401 (2021).
- [32] Brenden R. Ortiz, Samuel M. L. Teicher, Linus Kautzsch, Paul M. Sarte, Noah Ratcliffe, John Harter, Jacob P. C. Ruff, Ram Seshadri, and Stephen D. Wilson, arXiv:2104.07230.
- [33] Noah Ratcliff, Lily Hallett, Brenden R. Ortiz, Stephen D. Wilson, John W. Harter, arxiv: 2104.10138.
- [34] H. Miao, H. X. Li, W. R. Meier, H. N. Lee, A. Said, H. C. Lei, B. R. Ortiz, S. D. Wilson, J. X. Yin, M. Z. Hasan, Ziqiang Wang, Hengxin Tan, Binghai Yan, arXiv:2106.10150.
- [35] See supplementary information for raw data and additional discussion.
- [36] Zhengguo Wang, Sheng Ma, Yuhang Zhang, Haitao Yang, Zhen Zhao, Yi Ou, Yu Zhu, Shunli Ni, Zouyouwei Lu, Hui Chen, Kun Jiang, Li Yu, Yan Zhang, Xiaoli Dong, Jiangping Hu, Hong- Jun Gao, and Zhongxian Zhao, arXiv:2104.05556.
- [37] C. Mielke III, D. Das, J. -X. Yin, H. Liu, R. Gupta, C. N. Wang, Y. -X. Jiang, M. Medarde, X. Wu, H. C. Lei, J. J. Chang, P. Dai, Q. Si, H. Miao, R. Thomale, T. Neupert, Y. Shi, R. Khasanov, M. Z. Hasan, H. Luetkens, Z. Guguchia, arxiv: 2106.13443.
- [38] Xilin Feng, Kun Jiang, Ziqiang Wang, and Jiangping Hu, *Science Bulletin* **66**, 1384 (2021).
- [39] Yu-Ping Lin and Rahul M. Nandishore, *Phys. Rev. B* **104**, 045122 (2021).